PRELIMINARY STABILITY ANALYSIS OF THE CFETR CENTRAL SOLENOID CONDUCTORS

HUAN WU,* YUNTAO SONG, XUFENG LIU, SHUANGSONG DU, XIANG JI,
KAIZHONG DING, JINXIANG ZHENG, SUMEI LIU, and KUN LU

*Institute of Plasma Physics, Chinese Academy of Sciences, 350 Shushanhu Road, Hefei
Anhui 230031, China*

A central solenoid (CS) conductor layout has been tentatively decided during the conceptual design phase of the Chinese Fusion Engineering Testing Reactor (CFETR). To check the validity of the conductor layout, stability analysis must be performed against the working condition of the conductors. We constructed a superconducting critical surface of the strands used in the CS conductors and then calculated the current sharing temperature of the conductors under the most stringent working condition envisioned with the operation parameters. We further analyzed the energy margin by simulating the quenching behavior with the GANDALF code upon disturbances of different durations and lengths representative of a mechanical disturbance and plasma disruption. The analysis results give preliminary estimation of conductor stability for further improvement of the design.

KEYWORDS: *CFETR central solenoid, cable-in-conduit conductor, stability*

Note: Some figures in this paper may be in color only in the electronic version.

I. INTRODUCTION

The Chinese Fusion Engineering Testing Reactor (CFETR) has been proposed to bridge the gap between ITER and the demonstration fusion power plant (DEMO) to ultimately realize fusion energy applications in China. As it is complementary to ITER and has a more ambitious goal in terms of duty cycle time and tritium self-sustainability, CFETR will proceed with the ITER scientific base and engineering achievements to explore the power plant potential step by step in China. The main parameters of CFETR are summarized in Table I.

As the most important component of the CFETR machine, the tokamak magnet system consists of 16 toroidal field (TF) coils, 6 poloidal field (PF) coils, 6 central solenoid (CS) coils, and 24 correction coils (CCs); each coil has a similar function to its counterpart in the ITER machine.[1] Figure 1 is a conceptual illustration of the CFETR magnet system. Each CS coil of the magnet system is operated independently and built with six hexapancakes. Butt joints are located at the outermost turns to connect the pancakes, and overlap joints are used for the terminals. To cool the coils, supercritical helium is sent into the cooling channels in parallel through the helium inlets located at the innermost turns, and the helium exits from the outlets located at the outermost turns. While PF coils and CCs use NbTi cable-in-conduit conductors (CICCs), the CS and TF coils use Nb_3Sn CICCs.

The PF and CS coils are positioned symmetrically at both sides of the equator to form the PF system and to enable both single-null and double-null mode operation. The PF system design is optimized to meet both the equilibrium field and the ohmic heating field requirements. According to the physical design parameters, the poloidal field generated by CS and PF magnets must provide enough heating volt-second consumption to ensure that even in the exclusive ohmic heating condition,

---

*E-mail: hwu@ipp.ac.cn

TABLE I

Main Parameters of CFETR

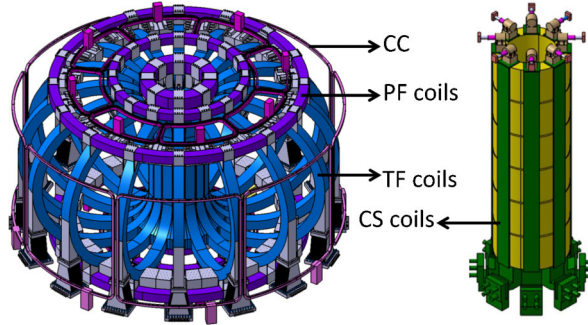|	
Plasma current, I_p (MA)	8.5/10
Major radius of plasma, R (m)	5.7
Minor radius of plasma, a (m)	1.6
Central magnetic field, B_t (T)	4.5/5.0
Elongation ratio, κ	1.8
Triangle deformation, δ	0.4

Fig. 1. Conceptual illustration of CFETR magnets.

plasma current of a certain duration can still be achieved. According to the current magnet structure design, this objective demands the conductors of the CS sustain a maximum current of 60 kA at 4.5 K in a maximum magnetic field of 14.965 T, of which 1.765 T is contributed by the PF coils. Based on these requirements, the CS conductor layout summarized in Table II is proposed tentatively.

Because of the limited heat capacity available as the heat sink after thermal perturbation, force-flow–cooled conductors have a limited stability margin.[2] For stable operation of the conductors, it is common practice to check the stability against adverse working conditions.[3–6] To assess the stability of the CFERT CS conductor for justification of the design, we carried out temperature margin and energy margin analysis based on the current conductor layout. As the related parameters for

TABLE II

CFETR CS Cable Layout

Strand	0.83 mm in diameter
Cabling configuration	$(2Sc + 1Cu) \times 3 \times 4$
	$\times 6 \times 6$ (864 Sc, 432 Cu)
Void fraction	30%
Central channel	9×10 mm in diameter
Cable	37.3 mm in diameter
Conductor	54.3×54.3 mm
Turn insulation thickness	2 mm

thermal-hydraulic analysis have not yet been determined in the conceptual design phase, a simulation to define the time and location of the minimum temperature margin for the stability analysis is not yet available. But, this does not stop us from carrying out preliminary stability analysis. We thus push the conductor working parameters to the most stringent limits and make a conservative analysis. The results are then compared with the design criteria of the ITER CS magnet to see if the current design is based on a sound engineering foundation.

II. SUPERCONDUCTING STRAND CRITICAL SURFACE

In 2008, Bottura and Bordini[7] compared a number of models for the critical surface of Nb_3Sn developed over the past years using consistent notation of normalized pinning force versus the reduced field and proposed a parameterization for the characterization and production follow-up of the ITER Nb_3Sn strands. This parameterization is defined by Eqs. (1) through (5):

$$J_c = \frac{C}{B} s(\varepsilon)(1-t^{1.52})(1-t^2)b^p(1-b^q) , \quad (1)$$

$$T_c(B,\varepsilon) = T_{c0max}[s(\varepsilon)]^{1/3}(1-b_0)^{1/1.52} , \quad (2)$$

$$B_{c2}(T,\varepsilon) = B_{c20max}s(\varepsilon)(1-t^{1.52}) , \quad (3)$$

$$s(\varepsilon) = 1 + \frac{1}{1-C_{a1}\varepsilon_{0,a}}\left[C_{a1}(\sqrt{\varepsilon_{sh}^2 + \varepsilon_{0,a}^2}\right.$$
$$\left. - \sqrt{(\varepsilon-\varepsilon_{sh})^2 + \varepsilon_{0,a}^2}) - C_{a2}\varepsilon\right] , \quad (4)$$

and

$$\varepsilon_{sh} = \frac{C_{a2}\varepsilon_{0,a}}{\sqrt{C_{a1}^2 - C_{a2}^2}} , \quad (5)$$

where

J_c = critical current

$T_c(B,\varepsilon)$ = critical temperature

$B_{c2}(T,\varepsilon)$ = critical field

$s(\varepsilon)$ = strain function

B = magnetic field

T = temperature

ε = strain

$b = B/B_{c2}(T,\varepsilon)$ = normalized field

$b_0 = B/B_{c2}(0,\varepsilon)$ = normalized field at a temperature of zero

$t = T/T_c(0,\varepsilon)$ = normalized temperature,

TABLE III

Reference Scaling Parameters for CFETR CS Strand

Parameter	Definition	Value
C (A·T/mm^2)	Scaling constant	18 700
B_{c20max} (T)	Upper critical field at zero temperature and strain	32.57
T_{c0max} (K)	Critical temperature at zero field and strain	17.17
p	Low field exponent of the pinning force	0.62
q	High field exponent of the pinning force	2.125
C_{a1}	Strain fitting constant	53
C_{a2}	Strain fitting constant	8
$\varepsilon_{0,a}$	Residual strain component	0.0097
ε_{max}	Tensile strain at which the maximum critical properties are reached	-0.003253075

and the other parameters are the scaling parameters defined in Table III. CFETR CS conductors will use the same strand as the ITER CS conductors, so the above parameterization is adopted to define the superconducting critical surface for further calculation.

The reference scaling parameters used in Eqs. (1) through (5) are summarized in Table III. C is determined to satisfy the following equation: J_c (12 T, 4.2 K, -0.25%) = 875 A/mm^2. With Eqs. (1) through (5) and the scaling parameters, we constructed a superconducting critical surface for further stability analysis using the GANDALF CICC stability analysis code.[8,9]

III. TEMPERATURE MARGIN

The temperature margin is the difference between the working temperature and the current sharing temperature of a conductor. Based on the critical surface of the strand, we first calculated the temperature margin of the conductors. In Sec. II, only the equation for J_c was defined explicitly. To calculate the current sharing temperature T_{cs}, the inverse of the J_c function was used; i.e., T_{cs} is the temperature at which the operation current density is just the critical current density.

The cooling helium inlets for the CS coils are located at the joggles of the innermost turns, while the outlets are located at the outermost turns.[1] The turns under the highest field in the CS are the innermost turns of each coil, as there is a field gradient across the winding pack. So, the temperature of the conductors under the highest field and also the highest strain due to electromagnetic forces scaled to the magnetic field is $\sim$4.5 K, i.e., the temperature of the helium at the inlets. As shown by the thermal-hydraulic simulation for the ITER CS, the conductor with the lowest temperature margin is located in the innermost turn where the temperature is close to the helium inlet temperature.[10] As the CFETR CS is of a similar structure to the ITER CS, we thus presumed that in the CFETR CS, the conductor of lowest temperature margin is located at the inlet. Based on this assumption,

we made calculations in the extreme condition where the field and strain are kept constant at the highest value, and the results are the following:

1. In a field of 14.965 T, and with a strain of -0.8%, the critical temperature of the conductors is 10.2 K.

2. In a field of 14.965 T, and with a strain of -0.8%, when the operating current is 60 kA, the current sharing temperature is 5.6 K.

3. At a helium inlet temperature of 4.5 K, in a field of 14.965 T, and with a strain of -0.8%, the critical current of the conductors is 81 kA.

4. The lower limiting current is the maximum allowable cable space current for operation in a well-cooled regime where the joule heat generation is lower than the heat transfer to the helium. It can be written as $I_{lim}^{low} = [A_{cu}p_w h(T_c - T_{cs})/\rho_{cu}]^{1/2}$, where A_{cu} is the cross section of the copper including the isolated copper strands, h is the heat transfer coefficient between the strands and helium, p_w is the wetted perimeter of the superconducting strands, and ρ_{cu} is the resistivity of copper at 4.5 K and 14.965 T. Taking h as 1000 W/m^2·K, we then have a lower limiting current of 72 kA.

Given that $T_{cs} = 5.6$ K in this condition, the lowest temperature margin is 1.1 K. The temperature margin of the conductor in turns other than the innermost one should be higher than 1.1 K. These results confirm that even in the extreme condition of -0.8% in strain and 14.965 T in field, the conductors of the current design layout can still carry 60 kA with an abundant redundancy of 12 kA to reach the lower limiting current.

IV. ENERGY MARGIN: MODEL AND BOUNDARY CONDITIONS

The energy margin is the maximum disturbance of the heat load that can be absorbed without leading to quenching by the conductor.[2] For a length of conductor,

the lowest energy margin under the most stringent condition in terms of the temperature margin is of significance. The CS coils work in the pulsed mode condition with a predefined conductor current scenario. For a complete energy margin analysis with the one-dimensional finite element code GANDALF, a thermal-hydraulic simulation to determine the boundary condition is needed. As this simulation is not available for the CFETR CS conductors in the conceptual design phase, we carried out energy margin analysis at the extreme condition where the field, strain, and current are kept constant at the highest value. In this condition, the energy margin would be conservative.

The input parameters used in GANDALF are summarized in Table IV. Note that some parameters, such as EPSLON, E0, NPOWER, and RRR, are based on parameters used in stability assessment of ITER conductors.[10–16] To use a finite element code for energy margin calculation, it is important to carefully choose the mesh size and time step to reach reliable results. For the meshing, we take advantage of the GANDALF functionality of adaptive meshes. The meshing parameters for the calculation are summarized in Table V. We chose adaptive meshing with initial local refinement in the region from XBREFI to XEREFI. A total of NELEMS elements are generated in the cooling path of length XLENGT, of which NELREF are in the refined region. The mesh is adaptive with minimum and maximum mesh sizes determined by the SIZMIN and SIZMAX parameters.

For the time step, if it is too long, the energy margin calculated could be lower than the real one because the temperature of the strand will rise suddenly due to the large heat flux loaded onto the strands during one time step. We thus investigated the relationship between the minimum allowed time step used by GANDALF and the stability margin result for a mechanical disturbance as an example to guide us to the proper time step. As shown in Table VI, the energy margin increases with time step starting from 1.0×10^{-3} s remarkably and finally saturates at 1.0×10^{-7} s. This verification determined the use of 1.0×10^{-7} s as the minimum allowed time step to ensure the calculation is carried out when the energy margin is the largest. As the plasma disruption takes place over an even longer period of 0.1 s than that of the mechanical disturbance, this minimum allowed time step of 1.0×10^{-7} s is suitable for both mechanical disturbances and plasma disruption.

TABLE IV

Input Parameters for GANDALF

Parameter	Value	Note
ASC (m^2)	233.74×10^{-6}	$A_{non-copper}$ in superconducting strand
AST (m^2)	233.74×10^{-6}	A_{copper} in superconducting strand
AJK (m^2)	1855.77×10^{-6}	Cross section of stainless steel jacket
AIN (m^2)	450.4×10^{-6}	Cross section of glass-epoxy insulation layer
ISC	-32	External routine defined by user according to Sec. II
IST	1	Copper
IJK	13	Stainless steel
IIN	22	Glass-epoxy
AHEB (m^2)	304.25×10^{-6}	A_{helium} in annulus
AHEH (m^2)	78.54×10^{-6}	A_{helium} in central tube
EPSLON	8.0×10^{-3}	—
E0 (V/m)	1.0×10^{-5}	—
NPOWER	7	—
RRR	100	—
DHB (m)	4.1212×10^{-4}	$4 \times A_{helium}$ in annulus/wetted perimeter of annulus
DHH (m)	10.0×10^{-3}	Outer diameter of the central tube
PHTC (m)	1.87742	Wetted perimeter of superconducting strands scaled with 5/6
PHTCJ (m)	1.17181×10^{-2}	Perimeter used for heat transfer calculation between strands and jacket, cable circumference/10
PHTJ (m)	1.05463×10^{-1}	Perimeter used for heat transfer calculation between the bundle helium and the jacket, cable circumference $\times$ 9/10
PHTHB (m)	31.42×10^{-3}	Perimeter used for heat transfer calculation between bundle helium and hole helium
PERFOR	0.1	Perforation of the separation perimeter between the bundle helium and the hole helium
TEMINL (K)	4.5	Temperature at inlet

TABLE V

Meshing Parameters

Parameter	Mechanical Disturbance	Plasma Disruption	Note
XLENGT (m)		200	Length of the cooling channel
NELEMS		9999	Number of elements in the mesh
ITYMSH		3	Adaptive with initial local refinement in the region from XBREFI to XEREFI
XBREFI (m)	97.5	75.0	Beginning of the initial refinement region
XEREFI (m)	102.5	125.0	End of the initial refinement region
NELREF		5000	Number of elements in the refined region
SIZMIN (m)	1.0×10^{-3}	1.0×10^{-2}	Minimum allowed element size used in the vicinity of the normal fronts
SIZMAX (m)	4.0×10^{-2}	4.0×10^{-2}	Maximum allowed element size

TABLE VI

Time-Step Dependence of Energy Margin*

Minimum Allowed Time Step (m)	Energy Margin (mJ/cm^3)
1.0×10^{-3}	111
1.0×10^{-4}	215
1.0×10^{-5}	233
1.0×10^{-7}	234

*Mechanical disturbance, temperature = 4.5 K, pressure = 6 bars, and mass flow rate = 8 g/s of helium at inlet.

V. ENERGY MARGIN: ANALYSIS RESULTS

Energy margins generated with the GANDALF code are summarized in Table VII. The combination of duration 0.001 s and length 0.01 m is representative of a mechanical disturbance, while that of 0.1 s and 10 m is representative of plasma disruption. For each given helium inlet pressure of 6, 7, and 8 bars, the energy margin is independent of helium mass flow rate in the range 8 to 12 g/s, and only a slight dependence on helium inlet pressure can be observed. Figures 2 and 3 show typical comparisons of the strand temperature distribution between recovery and quenching for both a mechanical disturbance and plasma disruption. The heat flux is applied at the middle of the conductor length.

For both mechanical and electromagnetic disturbances, all the margins generated with the GANDALF code are at least twice as large as 100 mJ/cm^3, which is the energy margin design criterion of ITER CS conductors.[10,11]

VI. CONCLUSION

Preliminary stability analysis shows that the lowest temperature margin of CFETR CS conductors of the current layout is 1.1 K, the energy margin for a mechanical disturbance is ~230 mJ/cm^3, while for plasma disruption, the energy margin is ~360 mJ/cm^3; these values are higher than the design criteria for ITER

TABLE VII

Energy Margins of Conductors

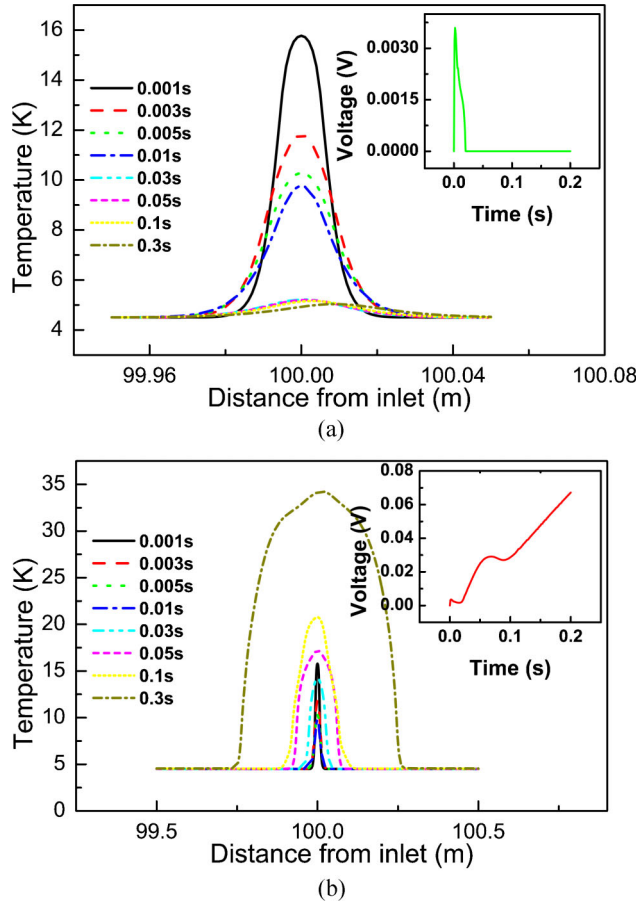| A_{strand} (m²) | 4.6748×10^{-4} |
|---|---|---|---|---|---|---|
| Duration (s) | 0.001 | | | 0.1 | | |
| Length (m) | 0.01 | | | 10 | | |
| Helium inlet pressure (bars) | 6 | 7 | 8 | 6 | 7 | 8 |
| External heat flux into strands (W/m) | 1.094×10^5 | 1.081×10^5 | 1.073×10^5 | 1661 | 1688 | 1715 |
| External energy (J) | 1.094 | 1.081 | 1.073 | 1661 | 1668 | 1715 |
| Energy margin (mJ/cm^3) | 234 | 231 | 230 | 356 | 361 | 367 |

(a)

(b)

Fig. 2. Strand temperature distribution when the conductor (a) recovers and (b) quenches after a mechanical disturbance. Insert panels show the corresponding voltage development over time. The temperature, pressure, and mass flow rate of helium at the inlet are 4.5 K, 6 bars, and 8 g/s, respectively. Heat flux is centered at 100 m from the inlet and applied at 0 s with a length of 0.01 m and a duration of 0.001 s.
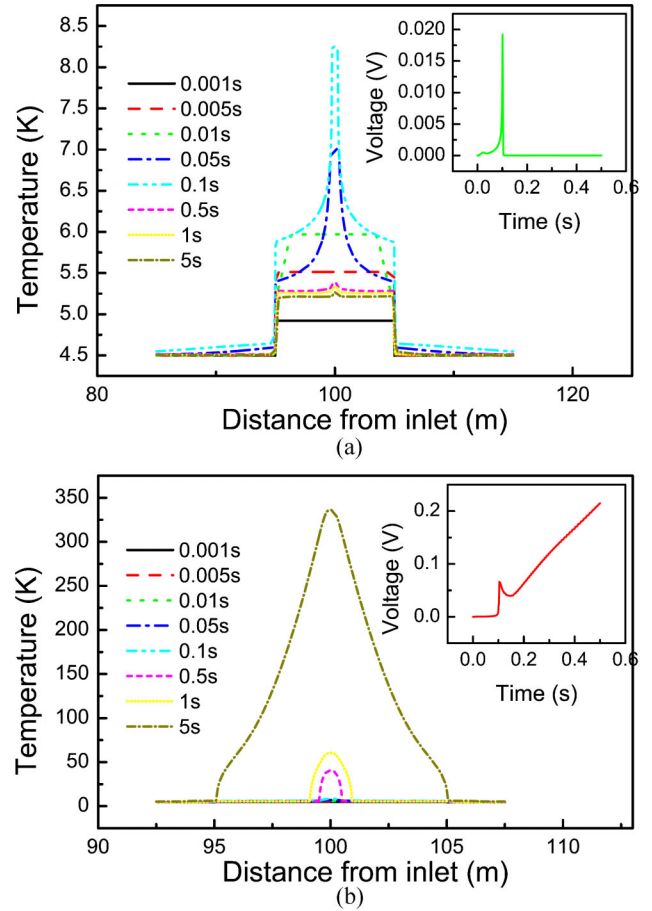

(a)

(b)

Fig. 3. Strand temperature distribution when the conductor (a) recovers and (b) quenches after plasma disruption. Insert panels show the corresponding voltage development over time. The temperature, pressure, and mass flow rate of helium at the inlet are 4.5 K, 6 bars, and 8 g/s, respectively. Heat flux is centered at 100 m from the inlet and applied at 0 s with a length of 10 m and a duration of 0.1 s.

CS conductors. Analysis results suggest that the stability of CFETR CS conductors of the current tentative layout is sufficient.

Regarding the observation of performance degradation of ITER CS conductors due to electromagnetic forces, further stability analysis is expected to be repeated with an improved model in consideration of new experimental observations. To carry out stability analysis with more precisely determined boundary conditions, a comprehensive thermal-hydraulic simulation is being planned.

ACKNOWLEDGMENTS

REFERENCES

1. CFETR TOKAMAK MACHINE DESIGN TEAM, "Report on Conceptual Design of CFETR Tokamak Machine," Technical Report, Institute of Plasma Physics, Chinese Academy of Physics (ASIPP) (2012).

2. L. BOTTURA, *Fusion Eng. Des.*, **20**, 351 (1993); http://dx.doi.org/10.1016/0920-3796(93)90065-P.

3. V. C. SRIVASTAVA, *Fusion Sci. Technol.*, **4**, 930 (1983).

4. N. MARTOVETSKY et al., *Fusion Sci. Technol.*, **44**, 19 (2003).

5. J. BALDZUHN et al., *Cryogenics*, **46**, 507 (2006); http://dx.doi.org/10.1016/j.cryogenics.2006.01.002.

6. J.-L. DUCHATEAU et al., *Fusion Sci. Technol.*, **64**, 705 (2013).

7. L. BOTTURA and B. BORDINI, *IEEE Trans. Appl. Supercond.*, **19**, 1521 (2009); http://dx.doi.org/10.1109/TASC.2009.2018278.

8. L. BOTTURA, *J. Comput. Phys.*, **125**, 26 (1996); http://dx.doi.org/10.1006/jcph.1996.0077.

9. L. BOTTURA, *Phys. C: Supercond.*, **310**, 316 (1998); http://dx.doi.org/10.1016/S0921-4534(98)00482-1.

10. L. S. RICHARD, D. BESSETTE, and R. ZANINO, *AIP Conf. Proc.*, **1218**, 668 (2010); http://dx.doi.org/10.1063/1.3422416.

11. C. MARINUCCI, L. SAVOLDI, and R. ZANNINO, *IEEE Trans. Appl. Supercond.*, **9**, 612 (1999); http://dx.doi.org/10.1109/77.783370.

12. Y. TAKAHASHI et al., *IEEE Trans. Appl. Supercond.*, **17**, 2426 (2007); http://dx.doi.org/10.1109/TASC.2007.899878.

13. L. S. RICHARD and R. ZANINO, *AIP Conf. Proc.*, **985**, 1269 (2008); http://dx.doi.org/10.1063/1.2908482.

14. L. RICHARD, D. BESSETTE, and R. ZANINO, *IEEE Trans. Appl. Supercond.*, **19**, 1496 (2009); http://dx.doi.org/10.1109/TASC.2009.2018752.

15. S. NICOLLET et al., *Cryogenics*, **49**, 687 (2009); http://dx.doi.org/10.1016/j.cryogenics.2009.04.003.

16. Y. ILYIN et al., *IEEE Appl. Supercond.*, **20**, 415 (2010); http://dx.doi.org/10.1109/TASC.2010.2041216.